Research Article | Vol. 28, No. 9 / 27 April 2020 / Optics Express 12837

Optics EXPRESS

Design, fabrication and characterization of a distributed Bragg reflector for reducing the étendue of a wavelength converting system

BOXUAN GAO,* JOHN PUTHENPARAMPIL GEORGE, JEROEN BEECKMAN, AND KRISTIAAN NEYTS

Electronics and Information Systems Department, Ghent University, Ghent, Belgium
boxuan.gao@ugent.be

Abstract: In this work, the design, fabrication and characterization are reported for a distributed Bragg reflector (DBR) filter with a specific wavelength and angular dependency, which aims to improve the light collection from a wavelength-converter-based light source into a smaller angle than the full angle Lambertian emission. The desired design is obtained by optimizing the transmission characteristics of a multi-layer structure. Titania (TiO_2) and silica (SiO_2) are used as high and low refractive index materials, respectively. The deposition is made by electron beam evaporation without substrate heating, followed by a post-annealing procedure. The optical properties of the evaporated layers are analyzed by ellipsometer and spectrometer measurements. The angular and wavelength dependency of the fabricated DBR is in good agreement with simulations for the designed structure.

1. Introduction

The amount of collected light from a light source is critical for many optical systems, such as projection display systems, because the image quality and the viewing experience are significantly influenced. A second essential parameter of the light source is the étendue, the product of the area and the solid angle of the emission. Reducing the étendue while maintaining the amount of collected light allows to reduce the size of optical systems. A reduction of étendue can be realized by concentrating light into a smaller cone angle, compared to Lambertian emission. An additional advantage of a smaller emission angle is that the collimation of light with conventional lenses becomes more efficient. This work focuses on a wavelength conversion system [1] that transforms incident blue light into green light, if possible with a small étendue. In this approach it is especially preferred to reduce the solid angle of the emission, because a larger emission area allows to reduce the power density and increase the conversion efficiency. For the considered wavelength conversion element, a reduced solid cone angle can be achieved by adding a well-designed optical filter that reflects light emitted at larger angles.

A distributed Bragg reflector (DBR) is a multi-layer structure with alternate layers of high and low refractive indices n_h and n_l, which are typically wavelength dependent. The wavelength range with high reflectivity, called the stop band, results from constructive interference of light reflecting on multiple interfaces. For high reflectivity around a central wavelength λ_c for perpendicular incidence, the layer thicknesses should be $d_i = \lambda_c/4n_i$, with n_i the corresponding refractive index. In this case, the peak reflectivity [2] is given by :

$$R_{HR,max} = \left(\frac{1 - (\frac{n_s}{n_a})(\frac{n_h}{n_l})^{2N}}{1 + (\frac{n_s}{n_a})(\frac{n_h}{n_l})^{2N}} \right)^2 \tag{1}$$

Where n_s is the refractive index of the substrate, n_a that of the surrounding ambient (air), and N is the number of repeated pairs of high and low refractive index layers. It can be seen

#391080 https://doi.org/10.1364/OE.391080
Journal © 2020 Received 26 Feb 2020; revised 10 Apr 2020; accepted 10 Apr 2020; published 15 Apr 2020

Optics EXPRESS

that increasing the number of layers and the contrast between the refractive indices, increases the reflectivity. In this way a peak reflectivity exceeding 99% can be achieved for a particular wavelength [3].

DBRs can be fabricated using different types of materials, for example organic polymers [4], semiconductors [5] or metal derivatives [6,7]. Different processes can be used to deposit DBR layers, such as chemical vapor deposition [8,9], sol-gel [10,11], sputtering [5,7] and electron-beam evaporation [12–14]. Due to their high reflectivity and low losses, DBRs have been widely used in many areas like optical filters [15], micro-cavities [7,16], vertical-cavity surface-emitting lasers [17], photonic crystals [18], organic light emitting diodes [19] and enhancement of emitting efficiency [20,21]. However, a current limitation of the DBR is that only the high reflection under a near-normal incidence is considered, also in a limited wavelength interval. The transmission property and the oblique incidence are often not taken into account. Still, more complex designs and applications are possible, as will be shown later.

In this work, a specific DBR is designed and fabricated as an optical filter with both wavelength and angular dependency, located in close proximity of a wavelength conversion material deposited on a reflector as shown in Fig. 1. The DBR filter should allow the excitation beam for the wavelength converter to pass, while only the emission of the wavelength-converter within a certain emission cone angle should be transmitted. The light that is emitted outside of this cone should be reflected by the DBR. As the emission material present here is a very strong scatterer [22], the reflected light will be back-scattered, again with a Lambertian distribution. After every scatter process there is a chance that the redistributed light is falling into the smaller emission cone. Ideally, after a few reflections most of the light should be emitted within the desired cone and be transmitted through the DBR. The requirements for the wavelength and angular dependency of the filter are as follows: it should have a high transmission for the blue excitation light (450 nm$<\lambda<$460 nm) within the incident cone angle ($\theta<22°$); a high transmission for the emitted green light (500 nm$<\lambda<$590 nm) within the incident cone angle ($\theta<45°$); and a high reflection for the same emitted green light (500 nm$<\lambda<$590 nm) outside of the incident cone angle ($\theta>45°$). This setup with a blue exciting beam and a photoluminescent emitter can be used when a large flux of green light is required with a small étendue (small area and small emission cone). In projection applications a dichroic mirror is used to split the exciting blue beam and the generated green beam, so that the green light can be combined with red and blue sources to generate white light. This principle is also relevant for directional phosphors used for high power LEDs [23]. Plane wave optical simulations for the transmission on a multi-layer structure have been carried out to determine the optimal DBR structure.

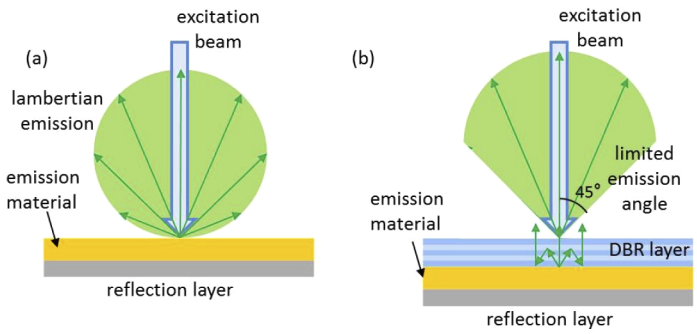

Fig. 1. Wavelength conversion set-up with a blue excitation beam and a green emission beam. (a) Lambertian emission by the emission material.(b) Emission with the DBR reflecting light outside of a certain cone angle. Light reflected by the DBR is scattered by the emission layer.

Optics EXPRESS

For the realization of this device, titania (TiO_2) and silicon dioxide (SiO_2) are chosen because of the large refractive index contrast and the stability of the materials [11,16]. It is well-known that untreated evaporated TiO_2 often suffers from strong absorption in the visible wavelength range [13] and has a refractive index lower than the reported crystalline value [18], thus it is essential to establish a proper post-annealing procedure. In this work, SiO_2 and TiO_2 are deposited by electron beam evaporation on unheated substrates without additional oxygen ambient. This is followed by an annealing step in a tube furnace with added oxygen to reduce the absorption in visible light by TiO_2 [24]. The angle and wavelength dependency of the transmission of the fabricated DBR is measured and compared to the numerical simulations.

In this work, we present a wavelength-selective thin film optical filter, realized by this specially designed and fabricated DBR, to be used in combination with a wavelength-converting-element to increase the light emitted within a given solid angle, and improve the conversion efficiency to transform incident blue light into collected green light.

2. Materials and methods

To prove the stability of the materials and the fabrication method, a simple DBR is made to compare between the simulation and experiment results. Si wafers and glass substrates are cleaned in ultrasonic baths with subsequently aceton, isopropanol and deionized water, on which the layers are deposited by e-beam evaporation in vacuum without substrate heating. The deposition rate and total thickness are monitored by a quartz crystal sensor, which measures the change in resonance frequency [25]. After each deposition of TiO_2, a post-annealing treatment in oxygen environment is carried out. In Figs. 2(a) and (b) a significant improvement in transparency by annealing is clearly visible for a single, 162 nm thick layer of TiO_2.

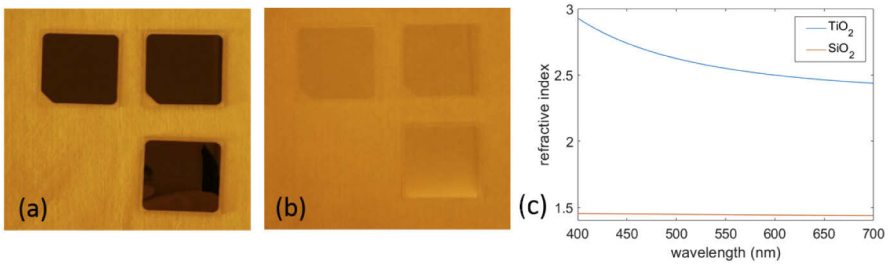

Fig. 2. Materials properties after post-annealing procedure. (a) and (b), transparency of a 162 nm thick TiO_2 layer before and after annealing, observed on a white background in yellow ambient light. (c) Real part of the refractive indices for TiO_2 (blue) and SiO_2 (red) extracted from ellipsometer data.

Samples with a single layer of TiO_2 or SiO_2 on silicon substrates have been fabricated and annealed for calibration purposes. From ellipsometer measurements, the layer thicknesses and the real part of the refractive indices have been extracted. The refractive indices as a function of wavelength for the fabricated TiO_2 and SiO_2 are shown in Fig. 2(c).

The transmission spectrum of a single layer of TiO_2 on glass is measured by a Perkin Elmer Lambda 35 UV/VIS spectrometer for wavelengths between 400 nm and 1000 nm. The obtained transmission spectrum is compared with the simulated one, based on the corresponding refractive index and thickness extracted from the ellipsometer. The result is shown in Fig. 3(a).

The good correspondence between measurement and simulation indicates that the thickness and the refractive index of the layer are similar to the values used in the simulation. For the blue region the measured transmission is lower than the simulated value, which indicates that there is some residual absorption in TiO_2.

Optics EXPRESS

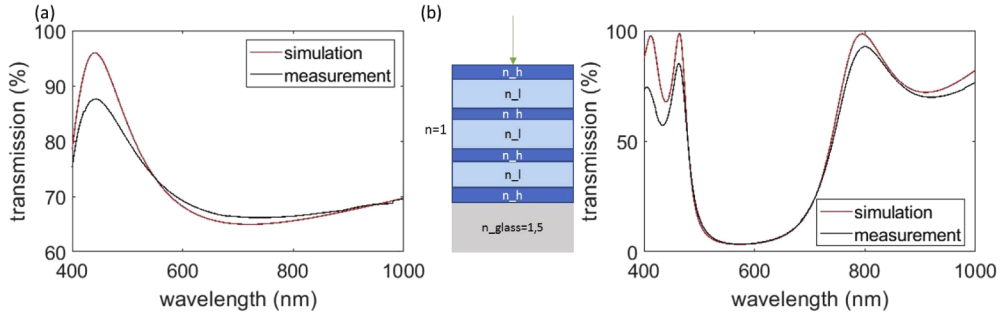

Fig. 3. Comparison between simulated and measured transmission spectra. Transmission spectra for (a) a single layer of TiO_2, and (b) a seven-layer DBR obtained from numerical simulation (red) and from measurement (black).

For the fabrication of a DBR, the annealing procedure is repeated, after each deposition of TiO_2. The thicknesses for the TiO_2 and SiO_2 layers are 63 nm and 105 nm respectively, corresponding to a maximum reflection at 630 nm. This DBR has 4 layers of TiO_2 and 3 layers of SiO_2, thus the structure can be described as $n_a/(n_h/n_l) \times 3/n_h/n_s$, with n_a the refractive index of air (=1) and n_s that of the substrate. The additional high refractive index layer leads to the highest reflectivity [26]. The simulated transmission and the measured transmission, together with the schematic structure of the DBR are shown in Fig. 3(b).

The measurement and simulation curve match well, indicating that the fabricated device operates as expected, and illustrating the reliability of the deposition procedure and the extracted material parameters.

3. DBR design and simulation

3.1. Objective and parameters

In this simulation, the DBR is designed to function as an optical filter to increase the transmission efficiency of the light excited from a Lambertian emitter. In the green range (from 500 nm to 590 nm), the DBR should have low transmission for angle of incidence θ above 45°, and meanwhile high transmission for angle of incidence below 45°, which requires transparent material. A second requirement is that for a range in the blue spectrum (for example from 450 nm to 460 nm), the transmission for angle of incidence below 22° should be high. The objectives for the transmission function $T(\lambda, \theta)$ are depicted in a wavelength-angle diagram in Fig. 4(a).

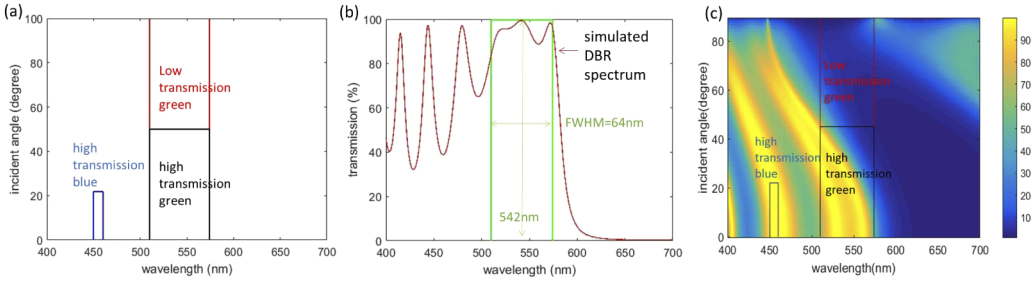

Fig. 4. Transmission property for the designed DBR. (a) Target regions in the wavelength-angle diagram. (b) Transmission spectrum of the DBR for normal incidence after the first iteration. The green range indicates the FWHM of the spectrum. (c) Transmission property of the designed eleven-layer-DBR, with indication of the three target regions.

Optics EXPRESS

In order to obtain a well-defined optimization of the DBR design, a figure of merit is proposed, taking into account the requirements for the different wavelength ranges.

As the blue spectral range for high transmission is narrow, we will only consider the middle of the wavelength interval, namely 455 nm. The average transmission within the cone with half angle 22° is defined by Eq. (2).

$$T_{blue} = \frac{\int_0^{22^\circ} T(455\text{nm}, \theta)\, sin(\theta)\, d\theta}{\int_0^{22^\circ} sin(\theta)\, d\theta} \tag{2}$$

For the green transmission range, we define the wavelength- dependent figure of merit F(λ) as the ratio of the average transmission within the cone θ<45° over the average transmission out of the cone (with θ>45°), as expressed by Eq. (3). To factor in the Lambertian distribution of emission and scattering, a cosine theta dependency has to be added to the weighing function.

$$F(\lambda) = \frac{\int_0^{45^\circ} T(\lambda, \theta) cos(\theta) sin(\theta)\, d\theta}{\int_{45^\circ}^{90^\circ} T(\lambda, \theta) cos(\theta) sin(\theta)\, d\theta} \tag{3}$$

A general green spectrum P(λ) is considered as the target, with wavelength range between 500 nm and 590 nm, full width half maximum (FWHM) of 64 nm with a central wavelength at 542 nm, as given in Fig. 4(b).

For a particular wavelength, the ratio of the light that is transmitted through the DBR towards the collecting lens, divided by the total transmission is given by F/(1+F). The figure of merit G, the efficacy of the light emitted towards the collecting lens, is then given by T_{blue} from Eq. (2), multiplied by the factor F/(1+F) weighted with the spectral density P(λ) of the emission from the layer, as shown in Eq. (4). When there is no DBR, this figure of merit G equals to 0.5 because the factor F becomes equal to one for all wavelengths under the condition of Lambertian emission.

$$G = \frac{\int_{\lambda_1}^{\lambda_2} \frac{F(\lambda)}{1+F(\lambda)} P(\lambda)\, d\lambda}{\int_{\lambda_1}^{\lambda_2} P(\lambda)\, d\lambda} \times T_{blue} \tag{4}$$

3.2. Simulations and results

For a conventional DBR, high reflectivity is obtained for a certain wavelength λ when the layer thicknesses are equal to a quarter-wavelength for the corresponding refractive indices ($d_i = \lambda_c/4n_i$). In our case, high reflectivity is desired for a continuous green wavelength range, under the condition of the incident angle above 45°. To achieve high reflectivity with a certain inclination angle θ, the thickness of each layer should be increased according to:

$$d_i = \frac{\lambda}{4 n_i cos\theta_i} \tag{5}$$

The transmission T(λ, θ) for a given multi-layer stack is calculated in Matlab based on the scattering matrix method, taking into account the interference of plane waves due to partial reflections at all interfaces [27]. Each layer is defined by its (real) refractive index and its thickness.

The aim of this work is to optimize the target function defined in Eq. (4) for a stack of TiO_2 and SiO_2 on a glass substrate. Based on the high index contrast of these materials, it is known that a DBR with only seven layers can yield a high reflection. However we found that by increasing the number of layers to eleven, a more detailed design and a higher figure of merit for our application could be obtained. Adding again more layers in the DBR would increase the complexity of optimization and fabrication. As there are now in total eleven layers to be adjusted, it is important

Optics EXPRESS

to start the optimization from a realistic estimation. For the first estimation, the initial thicknesses (quarter wavelengths) are designed to obtain high reflectivity (and low transmission) around 550 nm with incident angle 60°. For normal incidence, the reflection around 550 nm will be low (high transmission).

As already seen in Fig. 3(b), in a simple DBR spectrum, the transmission peak is very narrow compared to the FWHM of the required green range (64 nm). To fulfill the requirements of high transmission for a broad green band at normal incidence, with a high reflection for a broad green band at inclined incidence, the transmission peak adjacent to the reflection band needs to be broadened, which can be achieved through varying the layer thickness during a first iteration. Figure 4(b) shows the resulting transmission spectrum for normal incidence after the first iteration. The figure shows indeed maxima around 550 nm. The corresponding thicknesses for each layer after the first iteration are shown in the second row in Table 1 (labeled as 'starting point'). For this DBR stack, the calculated value of G is 0.3, which is low because in the first iteration we only aimed at increasing the transmission for normal incidence.

Table 1. Design parameters of the DBR after the first iteration ('starting point') and after the optimization of G ('final optimized'). All thicknesses are in nm.

	TiO_2 (air side)	SiO_2	TiO_2	SiO_2	TiO_2	SiO_2	TiO_2	SiO_2	TiO_2	SiO_2	TiO_2	G	T_{blue}
starting point	186	128	64	125	64	128	64	131	64	128	186	0.3	40.4%
final optimized	73.3	133.9	58.2	153.9	42.8	135.0	47.4	166.5	44.5	150.8	65.5	0.85	99.86%

Taking the values obtained after this first iteration as a starting point, the DBR thicknesses are further adjusted to optimize the figure of merit G mentioned above. For a DBR with m layers, this requires to find the optimized G value in an m-dimension space, where the variables are the thicknesses of the m layers.

To find the 11 layer thicknesses that maximize the value of G, a gradient method is implemented in an eleven-dimensional space. For each layer i, the difference in G is calculated when the thickness of this layer is incremented with a small amount Δd (e.g. 1 nm) as in Eq. (6). The gradient method provides the direction of steepest ascent to maximize the value of G. Equation (7) is used to adjust the different layers, where $\Delta d'$ determines the magnitude of the thickness change. After a number of iterations, in which the step size $\Delta d'$ is gradually reduced, the optimized set of layer thicknesses and corresponding value of G are found.

$$gradG_i = \frac{G(d_{old,i} + \Delta d) - G(d_{old,i})}{\Delta d} \tag{6}$$

$$d_{new,i} = d_{old,i} + \Delta d' \times \frac{gradG_i}{||gradG||} \tag{7}$$

For a DBR with 11 layers, the optimized thicknesses after this procedure are given in the third row of Table 1, labeled as 'final optimized'. The angle and wavelength dependency of the transmission is shown in Fig. 4(c). The corresponding factor G is equal to 0.85 and T_{blue} is equal to 99.86%. This is a considerable improvement from the starting point. Compared with the case without the DBR where G equals to 0.5, the efficacy of the emission light is increased by 70%.

4. Device fabrication and discussion

A device has been fabricated according to the design of Table 1 with eleven layers of TiO_2 and SiO_2, following the procedure described in section II. It is important to deposit the layers with accurate thicknesses in order to obtain a precise result. A cross section SEM image is shown in

Optics EXPRESS

Fig. 5, with the darker regions corresponding to TiO_2 layers. The measured spectrum for normal incidence is compared with the simulated transmission spectrum in Fig. 6(a). The match between the two curves indicates that the fabricated parameters are sufficiently accurate.

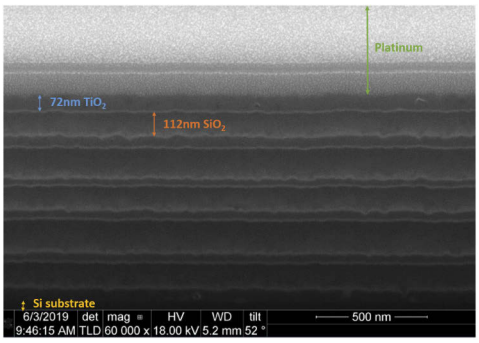

Fig. 5. Cross-sectional SEM image of the fabricated 11 layer DBR and measured thicknesses for the top two layers. The measured thicknesses in this image have limited accuracy due to thickness variations and the oblique side view of the SEM.

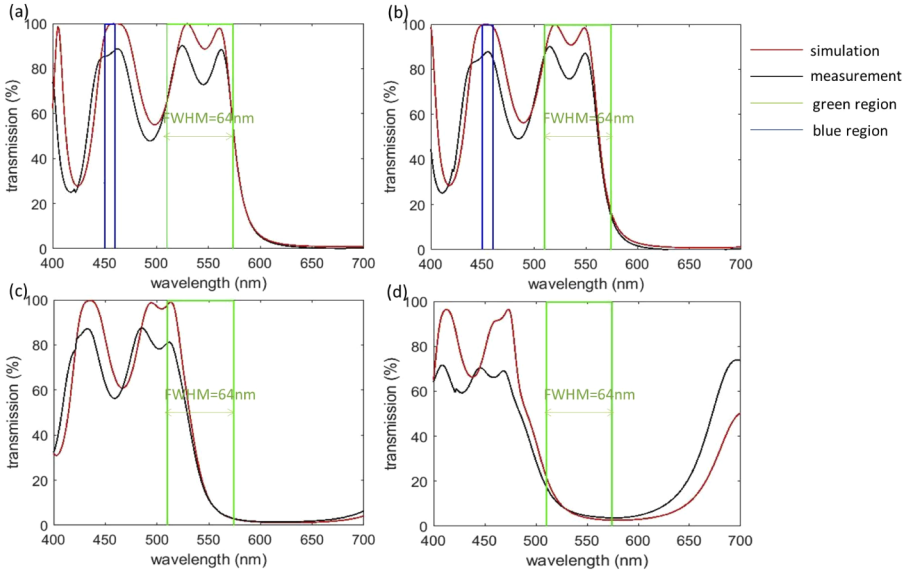

Fig. 6. Experimental and simulated transmission spectra (400 nm to 700 nm) of the fabricated DBR for different angles of incidence (a) normal incidence (b) θ =20° (c) θ =40° (d) θ =60°. The reduction in the measured transmission under large incident angle is caused by the reflection of the compensating glass substrate in the holder.

To realize the function of concentrating Lambertian emission into a small solid angel cone, different reflection and transmission properties are required under oblique incidence. Spectral transmission measurements for different inclination angles are conducted with a spectrophotometer with a holder designed for oblique incidence, which contains two rotatable sample holders. As the test sample holder is oriented under a certain angle, a second glass substrate under the opposite angle is used to compensate the lateral displacement caused by the inclined test sample. The spectra of the simulated and experimental results are plotted in the same graph together with the

Optics EXPRESS

target blue and green region, as shown in Fig. 6, where the measured and simulated spectra are highly corresponding. With the increase in inclination angle, the transmission window shifts to shorter wavelengths, as expected from the theory. For the green wavelength range of interest, the emission within a certain solid angle cone (around 40°) will be mostly transmitted through the DBR as it is in the transmission window. The emission out of the cone will be reflected back, as shown in Fig. 6(d), and get a another chance to be redirected into the cone. In this way, the Lambertian emitted light will be concentrated into a certain cone, thus increasing the transmission efficiency in this system. Note that the measured transmission is typically somewhat lower than the simulated value. This is partly due to the reflection at the glass/air interface, which is not taken into account in the simulations. In addition there may be a small amount of absorption or scattering in the experimental samples.

Figure 7 shows photographs of the fabricated device under different viewing angles. The color shift in transmission from green to blue and purple is clearly visible. The images show that the background image is not subjected to blurring, indicating that low-angle scattering is limited.

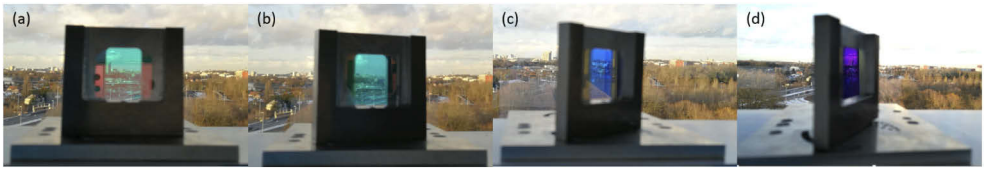

Fig. 7. Images of the fabricated sample observed under different angles with the city of Ghent in the background (a) normal view with green transmission; (b) 20° inclination with green transmission; (c) 40° inclination with blue transmission; (d) 60° inclination with purple transmission.

5. Conclusion

In this work the design and realization of a complex eleven-layer DBR filter with a particular angular and wavelength dependency is demonstrated. The figure of merit is defined to increase the light output for a wavelength converter over a given wavelength range and within a given emission cone. The DBR is based on TiO_2 and SiO_2 layers to realize respectively the high and low refractive index, and the materials are properly handled for precise optical properties. The deposition is conducted by e-beam evaporation in vacuum without substrate heating. A post-annealing procedure is used to reduce absorption in the TiO_2 layer and to obtain high transmission. The large refractive index contrast makes it possible to obtain a broad stop band with high reflectivity with only eleven layers. A particular design with specific requirements is optimized based on the gradient method. The resulting DBR stack has been fabricated by e-beam evaporation. Comparison between simulated and measured transmission spectra, at different inclination angles, indicates that the DBR operates according to the design. Green light is well transmitted for inclination angles below 45°, and well reflected for inclination angles above 45°. Blue light ranges from 450 nm to 460 nm is well transmitted for inclination angles below 22°. The simulated figure of merit G for the designed filter is 0.85 for this specific design. The realization indicates not only that the materials and the fabrication procedures are very promising, but also that DBR devices can be realized with a complex functionality.

Funding

Agentschap Innoveren en Ondernemen (HBC.2017.0141 MICROPRO).

Optics EXPRESS

Disclosures

The authors declare no conflicts of interest.

References

1. K. A. Denault, M. Cantore, S. Nakamura, S. P. DenBaars, and R. Seshadri, "Efficient and stable laser-driven white lighting," AIP Adv. **3**(7), 072107 (2013).
2. C. Sheppard, "Approximate calculation of the reflection coefficient from a stratified medium," Pure Appl. Opt. **4**(5), 665–669 (1995).
3. M. Muallem, A. Palatnik, G. D. Nessim, and Y. R. Tischler, "Room temperature fabrication of dielectric bragg reflectors composed of a caf2/zns multilayered coating," ACS Appl. Mater. Interfaces **7**(1), 474–481 (2015).
4. A. Convertino, A. Valentini, and R. Cingolani, "Organic multilayers as distributed bragg reflectors," Appl. Phys. Lett. **75**(3), 322–324 (1999).
5. E. Afsharipour, B. Park, and C. Shafai, "Determination of reactive rf-sputtering parameters for fabrication of siox films with specified refractive index, for highly reflective siox distributed bragg reflector," IEEE Photonics J. **9**(1), 1–16 (2017).
6. S. Y. Choi, M. Mamak, G. Von Freymann, N. Chopra, and G. A. Ozin, "Mesoporous bragg stack color tunable sensors," Nano Lett. **6**(11), 2456–2461 (2006).
7. S. Valligatla, A. Chiasera, S. Varas, N. Bazzanella, D. N. Rao, G. C. Righini, and M. Ferrari, "High quality factor 1-d er 3+-activated dielectric microcavity fabricated by rf-sputtering," Opt. Express **20**(19), 21214–21222 (2012).
8. K. Waldrip, J. Han, J. J. Figiel, H. Zhou, E. Makarona, and A. Nurmikko, "Stress engineering during metalorganic chemical vapor deposition of algan/gan distributed bragg reflectors," Appl. Phys. Lett. **78**(21), 3205–3207 (2001).
9. G. Huang, T. Lu, H. Yao, H. Kuo, S. Wang, C.-W. Lin, and L. Chang, "Crack-free ga n/ al n distributed bragg reflectors incorporated with ga n/ al n superlattices grown by metalorganic chemical vapor deposition," Appl. Phys. Lett. **88**(6), 061904 (2006).
10. R. M. Almeida and S. Portal, "Photonic band gap structures by sol–gel processing," Curr. Opin. Solid State Mater. Sci. **7**(2), 151–157 (2003).
11. S. Rabaste, J. Bellessa, A. Brioude, C. Bovier, J. Plenet, R. Brenier, O. Marty, J. Mugnier, and J. Dumas, "Sol–gel fabrication of thick multilayers applied to bragg reflectors and microcavities," Thin Solid Films **416**(1-2), 242–247 (2002).
12. G. Ma, J. Shen, K. Rajiv, S. Tang, Z. Zhang, and Z. Hua, "Optimization of two-photon absorption enhancement in one-dimensional photonic crystals with defect states," Appl. Phys. B **80**(3), 359–363 (2005).
13. L. Persano, P. D. Carro, E. Mele, R. Cingolani, D. Pisignano, M. Zavelani-Rossi, S. Longhi, and G. Lanzani, "Monolithic polymer microcavity lasers with on-top evaporated dielectric mirrors," Appl. Phys. Lett. **88**(12), 121110 (2006).
14. M. F. Schubert, J.-Q. Xi, J. K. Kim, and E. F. Schubert, "Distributed bragg reflector consisting of high-and low-refractive-index thin film layers made of the same material," Appl. Phys. Lett. **90**(14), 141115 (2007).
15. J. Dai, W. Gao, B. Liu, X. Cao, T. Tao, Z. Xie, H. Zhao, D. Chen, H. Ping, and R. Zhang, "Design and fabrication of uv band-pass filters based on sio2/si3n4 dielectric distributed bragg reflectors," Appl. Surf. Sci. **364**, 886–891 (2016).
16. Y. G. Boucher, A. Chiasera, M. Ferrari, and G. C. Righini, "Photoluminescence spectra of an optically pumped erbium-doped micro-cavity with sio2/tio2 distributed bragg reflectors," J. Lumin. **129**(12), 1989–1993 (2009).
17. B. Kogel, P. Debernardi, P. Westbergh, J. S. Gustavsson, A. A. Haglund, E. Haglund, J. Bengtsson, and A. Larsson, "Integrated mems-tunable vcsels using a self-aligned reflow process," IEEE J. Quantum Electron. **48**(2), 144–152 (2012).
18. G. Ma, J. Shen, Z. Zhang, Z. Hua, and S. H. Tang, "Ultrafast all-optical switching in one-dimensional photonic crystal with two defects," Opt. Express **14**(2), 858–865 (2006).
19. H. Antoniadis and D. B. Roitman, "Organic light emitting diodes with distributed bragg reflector," 2002, US Patent 6,366,017.
20. C. Chen, S.-J. Chang, Y.-K. Su, G.-C. Chi, J.-K. Sheu, and J.-F. Chen, "High-efficiency ingan-gan mqw green light-emitting diodes with cart and dbr structures," IEEE J. Sel. Top. Quantum Electron. **8**(2), 284–288 (2002).
21. H.-Y. Lin, K.-J. Chen, S.-W. Wang, C.-C. Lin, K.-Y. Wang, J.-R. Li, P.-T. Lee, M.-H. Shih, X. Li, H.-M. Chen, and H.-C. Kuo, "Improvement of light quality by dbr structure in white led," Opt. Express **23**(3), A27–A33 (2015).
22. M. Raukas, J. Kelso, Y. Zheng, K. Bergenek, D. Eisert, A. Linkov, and F. Jermann, "Ceramic phosphors for light conversion in leds," ECS J. Solid State Sci. Technol. **2**(2), R3168–R3176 (2013).
23. Y. Wang, Y. Wang, N. Chi, J. Yu, and H. Shang, "Demonstration of 575-mb/s downlink and 225-mb/s uplink bi-directional scm-wdm visible light communication using rgb led and phosphor-based led," Opt. Express **21**(1), 1203–1208 (2013).
24. V. Mikhelashvili and G. Eisenstein, "Effects of annealing conditions on optical and electrical characteristics of titanium dioxide films deposited by electron beam evaporation," J. Appl. Phys. **89**(6), 3256–3269 (2001).
25. A. Wajid, "On the accuracy of the quartz-crystal microbalance (qcm) in thin-film depositions," Sens. Actuators, A **63**(1), 41–46 (1997).

Optics EXPRESS

26. H. Baghdasaryan, T. Knyazyan, T. Baghdasaryan, B. Witzigmann, and F. Roemer, "Absorption loss influence on optical characteristics of multilayer distributed bragg reflector: wavelength-scale analysis by the method of single expression," Opto-Electron. Rev. **18**(4), 438–445 (2010).
27. L. Penninck, P. De Visschere, J. Beeckman, and K. Neyts, "Dipole radiation within one-dimensional anisotropic microcavities: a simulation method," Opt. Express **19**(19), 18558–18576 (2011).